Supporting information

Investigation of $AgGaSe_2$ as a wide gap solar cell absorber

Jes K. Larsen[1,*], Olivier Donzel-Gargand[1], Kostiantyn V. Sopiha[1], Jan Keller[1], Kristina Lindgren[2], Charlotte Platzer-Björkman[1], Marika Edoff[1]

[1] Division of Solar Cell Technology, Department of Materials Science and Engineering, Uppsala University, 75236 Uppsala, Sweden

[2] Division of Microstructure Physics, Department of Physics, Chalmers University of Technology, 41296 Göteborg, Sweden

*corresponding author: jes.larsen@angstrom.uu.se

1. XRD of reference materials

The XRD patterns of all the samples are compared to reference patterns of the target compound in the following.

1.1. XRD pattern of Ag_2Se

The literature pattern has the following properties [1]:

Space group: $P2_12_12_1$ (19), a=4.336 Å, b=7.070 Å, c=7.774 Å, α=90°, β=90°, γ=90°

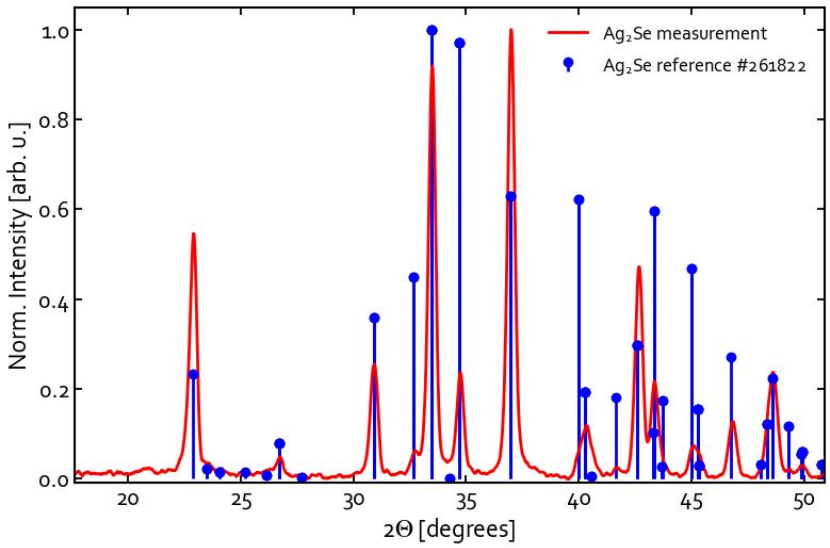

Figure S1: XRD pattern of the Ag_2Se thin film. The number in the legend refers to the ICSD FIZ Karlsruhe database collection code.

1.2. XRD pattern of Ag_9GaSe_6

The literature pattern has the following properties [2]:

Space group: $F\bar{4}3m$ (216), a=11.126 Å, b=11.126 Å, c=11.126 Å , α=90°, β=90°, γ=90°

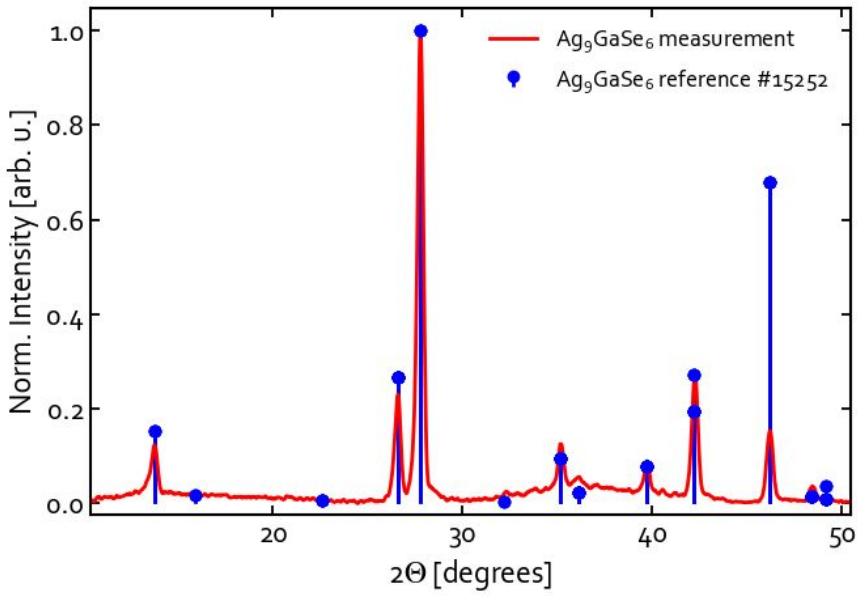

Figure S2: XRD pattern of Ag_9GaSe_6 thin film. The number in the legend refers to the ICSD FIZ Karlsruhe database collection code.

1.3. XRD pattern of $AgGaSe_2$

The literature pattern has the following properties [3]:

Space group: $I\bar{4}2d$ (122), a=5.993 Å, b=5.993 Å, c=10.884 Å, α=90°, β=90°, γ=90°

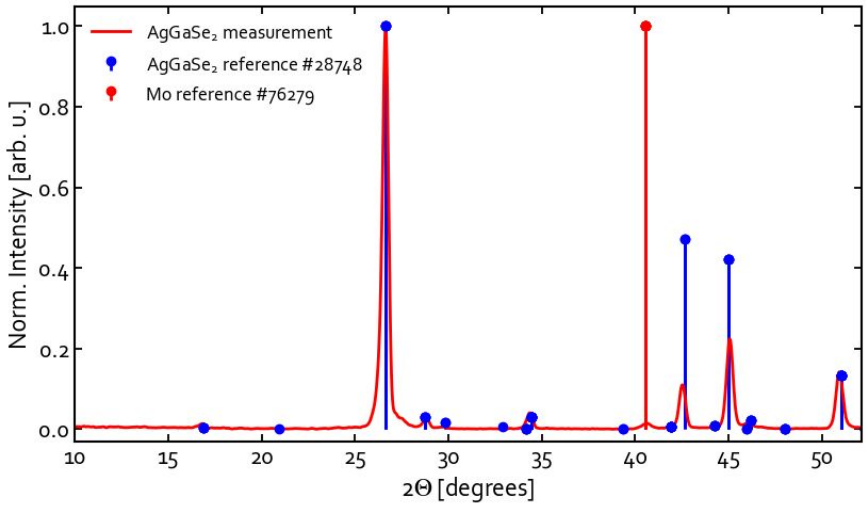

Figure S3: XRD pattern of $AgGaSe_2$ thin film on Mo. The number in the legend refers to the ICSD FIZ Karlsruhe collection code.

1.4. XRD pattern of Ga_2Se_3

The literature pattern has the following properties [4]:

Space group: C1c1 (9), a=6.66 Å, b=11.65 Å, c=6.64 Å, α=90°, β=108.84°, γ=90°

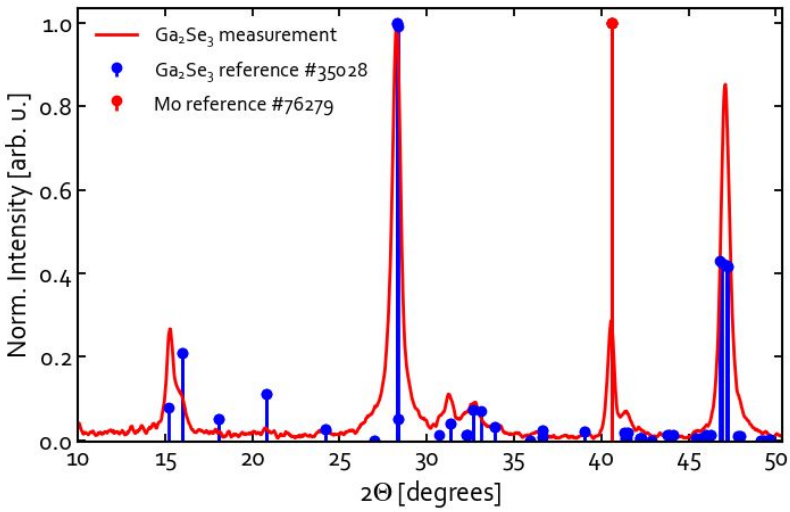

Figure S4: XRD pattern of Ga_2Se_3 thin film on Mo. The number in the legend refers to the ICSD FIZ Karlsruhe collection code.

1.5. XRD pattern of $AgGa_5Se_8$

The pattern of $AgGa_5Se_8$ has not been included in the International Centre for Diffraction Data database, but it has been reported in one study [5]. Ishizaki et al. refined the XRD pattern of $AgGa_5Se_8$ with a space group of P-42m and determined the lattice constants to be: a = 5.63 – 5.69 Å and c = 10.55 – 10.99 Å, with the exact values depending on the [Ag]/[Ga] ratio of the sample. In comparison, $AgIn_5Se_8$ has been found to have lattice constants: a = 5.79 Å and c = 11.62 Å [6]. The lattice constants found by Ishizaki et al. do not fit the pattern obtained for the sample in this study. Instead, we find that the measured pattern fits the reported lattice parameters of $AgIn_5Se_8$ when both lattice constants are reduced by 5%, that is: a = 5.50 Å and c = 11.04 Å. Figure S5 shows the measured diffractogram of the $AgGa_5Se_8$ sample in comparison with the simulated pattern. The main peaks fits the simulated OVC pattern well, with a small contribution from the chalcopyrite $AgGaSe_2$.

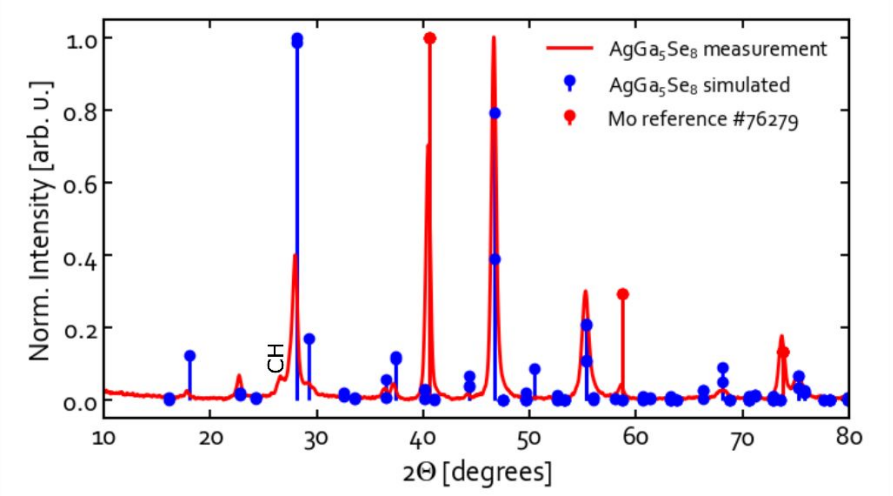

Figure S5: XRD pattern of $AgGa_5Se_8$ thin film on Mo. A small contribution from chalcopyrite $AgGaSe_2$ phase is marked "CH". The diffraction lines for $AgGa_5Se_8$ phase are extracted from a simulation on a model cell discussed above.

2. Optical properties of reference material samples

In order to estimate the band gap of the secondary phases, spectrophotometry was performed on the reference material samples deposited on soda-lime glass. Based on the recorded reflectance (R), transmittance (T), and film thickness (d), the absorption coefficients (α) were calculated according to the following:

$$\alpha = \frac{1}{d} ln\left(\frac{(1-R)^2}{T}\right)$$

The absorption spectra estimated with this approach are shown in Figure S6 (a) along with Tauc plots in Figure S6 (b).

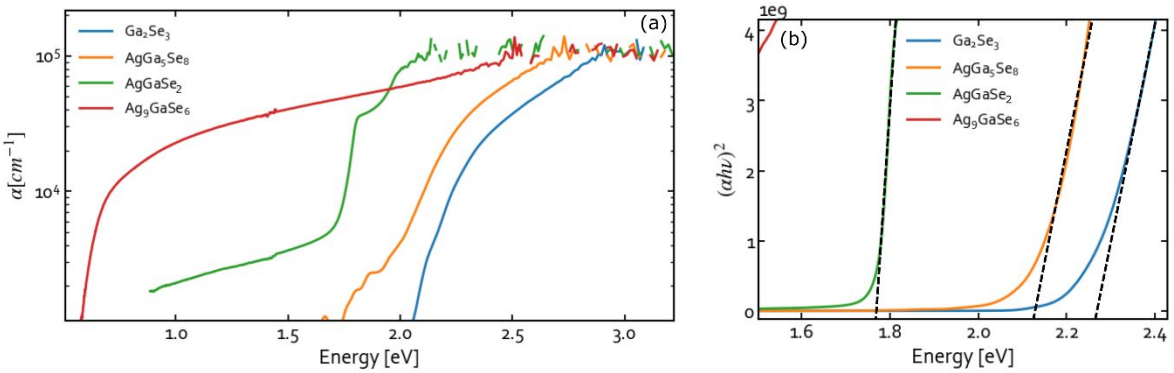

Figure S6: (a) Absorption coefficients of reference samples deposited on soda-lime glass and measured by spectrophotometry. (b) Tauc plots of absorption edges.

3. Raman spectra of reference samples

3.1. Raman spectrum of Ga_2Se_3

Figure S7 shows Raman spectra of Ga_2Se_3 collected with different laser wavelengths. The peaks at about 255 cm^{-1} and 295 cm^{-1} are particularly prominent with the 532 nm laser. The 255 cm^{-1} peak could originate from the presence of amorphous selenium (see discussion of $AgGaSe_2$ spectra).

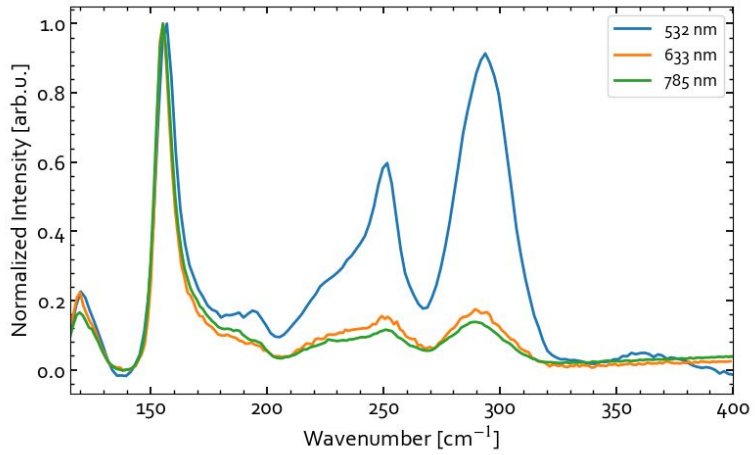

Figure S7: Raman spectra of Ga_2Se_3 reference sample measured with 532, 633, and 785 nm excitation wavelengths.

3.2. Raman spectrum of $AgGa_5Se_8$

Figure S8 shows Raman spectra of the $AgGa_5Se_8$ reference sample collected with different laser wavelengths. The spectra were collected in areas visually free from $AgGaSe_2$ particles on the film surface.

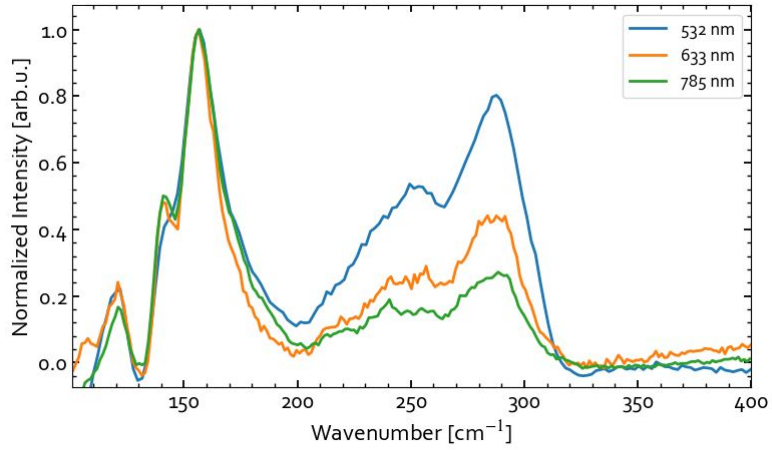

Figure S8: Raman spectra of $AgGa_5Se_8$ measured with 532, 633, and 785 nm excitation wavelengths.

3.3. Raman spectrum of $AgGaSe_2$

Raman measurements of $AgGaSe_2$ samples with different laser wavelengths, power densities, and exposure times revealed that this material is particularly prone to degradation. Similar results were obtained when measuring the $AgGaSe_2$ phase in samples grown with slightly Ag-poor to Ag-rich conditions. In order to demonstrate the difficulties encountered when performing Raman analysis, spectra of the Ag-poor sample grown via the 1-stage process (see main text) are included below.

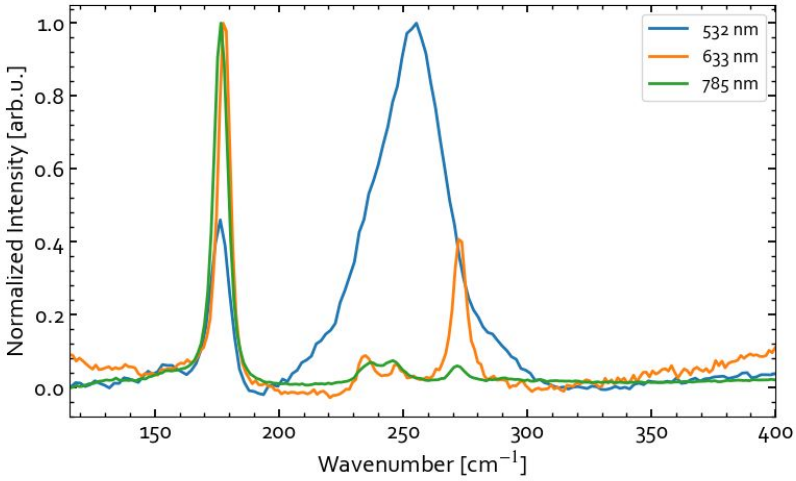

Figure S9: Raman spectra obtained with different laser wavelengths for the Ag-poor $AgGaSe_2$ sample produced via a 1-stage process.

Figure S9 shows the Raman spectra measured with various excitation wavelengths. With the 785 and 633 nm lasers, the peaks are observed at 178, 234, 247, and 273 cm^{-1}. These peaks are in decent good agreement with the Raman spectra previously published for $AgGaSe_2$ [7],[8].The spectrum obtained with the 532 nm laser is, however, different and shows a broad peak around 255 cm^{-1} along with the main peak of $AgGaSe_2$ at 178 cm^{-1}. This strong additional peak is not expected in $AgGaSe_2$. In order to investigate its origin, Raman measurements with various exposure times and excitation powers were performed.

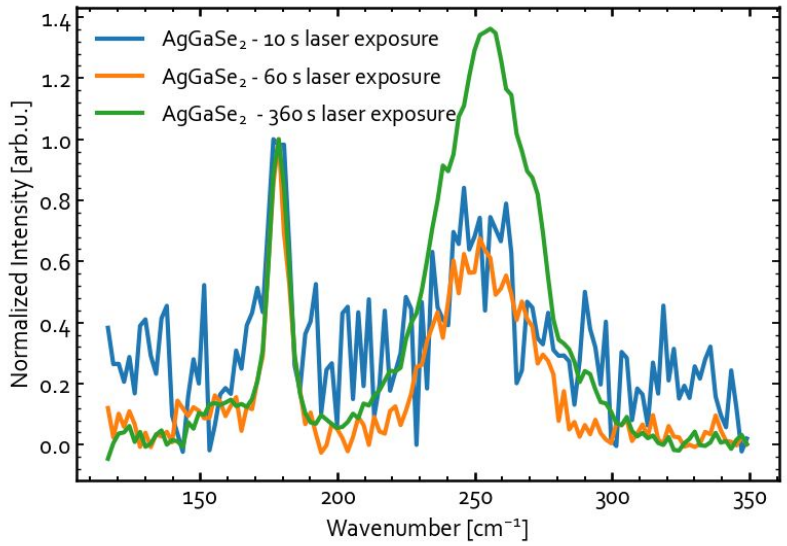

Figure S10: Raman spectra of the Ag-poor $AgGaSe_2$ sample grown with a 1-stage process normalized to the A1 mode. The excitation source is a 532 nm laser with about 5 W/cm^2 power density. The measurement was repeated on the same location with increasing acquisition time, resulting in in longer laser exposure time.

Figure S10 shows Raman spectra of $AgGaSe_2$ measured with the 532 nm laser and different exposure times. It is noticed that the peak at 255 cm^{-1} increases significantly in intensity relative to the A1 mode of $AgGaSe_2$ at 178 cm^{-1} with increasing exposure time. The fact that the spectrum changes rapidly even under conditions where the signal-to-noise ratio is low (see 10 s exposure time in Figure S10) makes it challenging to collect reliable high-quality data for these samples in air. This appeared to be especially problematic with 532 nm laser excitation.

Figure S11 illustrates the effect of increasing the power density on the Raman spectrum of $AgGaSe_2$. The 255 cm^{-1} mode increased even more significantly relative to the A1 mode in this case. The origin of this effect is not completely clear, but a possibility is that photoinduced redox reactions result in incorporation of oxygen and production of amorphous selenium at the surface. Photoinduced oxidation with formation of amorphous Se has been observed by Raman in epitaxial Ga_2Se_3 after one-hour exposure to a 514 nm laser with a power density of 380 W/cm^2 [9].The authors confirmed the oxidation by using Auger electron spectroscopy [9]. They proposed that the photoinduced oxidation result in formation of Ga_2O_3 and amorphous selenium at the sample surface.

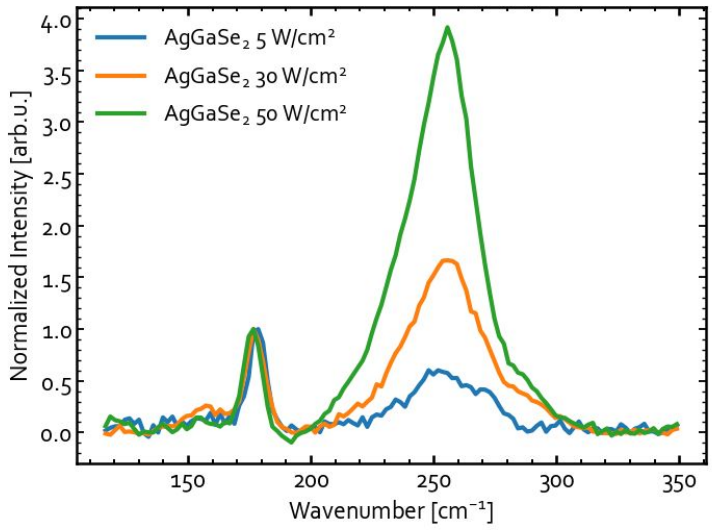

Figure S11: Raman spectra of the Ag-poor $AgGaSe_2$ sample grown with 1-stage process normalized to the A1 peak. Excitation with a 532 nm laser for 60 s with increasing laser power density from 5 to 50 W/cm^2.

To test if air exposure during measurements affects the 255 cm^{-1} peak, a couple of Raman spectra were acquired in a nitrogen atmosphere. This was done by placing the sample in a cryostat that was subsequently purged with N_2 prior to the measurement. The sample was again analysed with a 532 nm laser with a power density of about 5 W/cm^2. Two different exposure times were tested. Figure S12 compared the resulting Raman spectra in N_2 and air. It was observed that atmosphere does play an important role. In the N_2, the rapid growth of the 255 cm^{-1} peak was suppressed. This finding supports the hypothesis that oxidation of the surface is the cause for formation of amorphous Se. The results further highlights that $AgGaSe_2$ is extremely sensitive to laser exposure during Raman measurements, and that care must be taken to avoid photo-activated reactions.

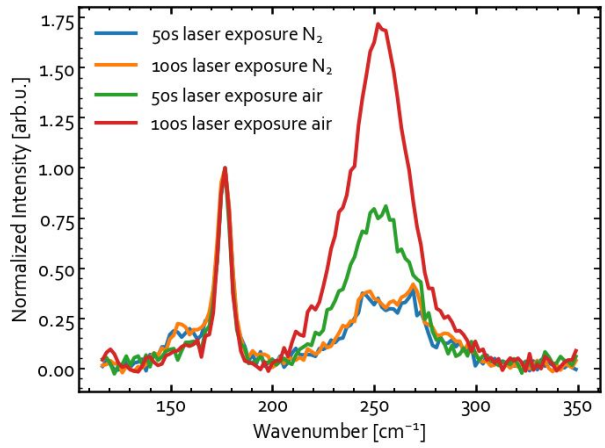

Figure S12: Comparison of Raman spectra of Ag-poor $AgGaSe_2$ sample grown with 1-stage process measured with 532 nm laser for different exposure times in N_2 atmosphere and air. The change in peak intensities is avoided in N_2 atmosphere.

3.4. Raman spectrum of Ag_9GaSe_6

It was attempted to acquire the Raman spectrum of Ag_9GaSe_6, since it is not available in literature. First attempts to measure the sample with low excitation power and short integration time (less than 10 W/cm^2, and shorter than 1 min) did not result in a signal with distinguishable peaks. It was therefore attempted to increase the laser power and integration time. The results are shown in Figure S13. A broad dominant peak centred around 254 cm^{-1} was observed with 532 nm excitation and a power of about 30 W/cm^2 and one-minute exposure. The peak at 178 cm^{-1} in Figure S13 is likely due to a small amount of $AgGaSe_2$ present in this sample. If longer laser exposure was used, another peak at about 237 cm^{-1} increased in intensity. By comparison to the Raman spectra of amorphous (a-Se)[10], and trigonal Se (t-Se)[11] deposited on SLG, it was realized that these signals are likely not the characteristic of Ag_9GaSe_6. It is instead proposed that the spectrum originates from a-Se for a shorter exposure time. After a few minutes, a-Se can partly crystalize to form t-Se. The crystallization of a-Se has previously been observed by illuminating a-Se with a 647 nm laser (100-1000 W/cm^2) for a few minutes [12]. It is likely that we observe the same phenomenon here. It is possible that a-Se on the sample surface could form due to photoinduced oxidation of Ag_9GaSe_6, akin to the effect observed in Ag-poor $AgGaSe_2$ above. An alternative explanation could be that a-Se was deposited on the surface during sample cool down.

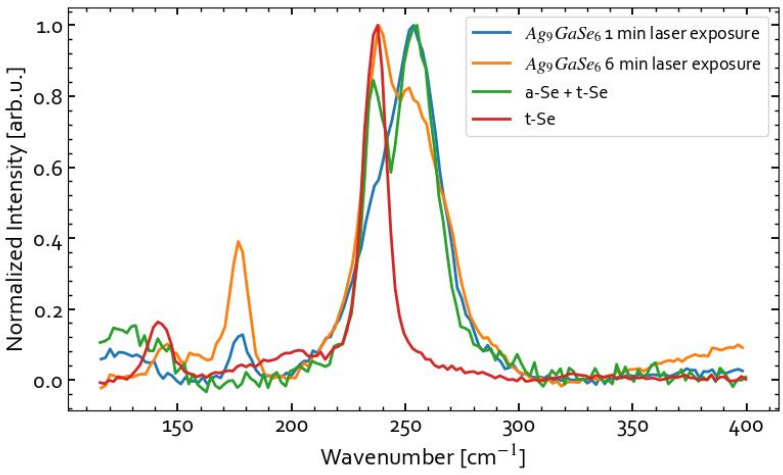

Figure S13: Raman spectra of the Ag_9GaSe_6 sample measured with 532 nm excitation with the laser exposure time of 1 minute (blue curve) and 6 minutes (orange curves). The results were acquired from the same spot. Reference Raman spectra of trigonal selenium (red curve)

4. Electrical properties of reference samples

In order to investigate the electrical properties of the reference materials, thin films were deposited directly on the soda-lime glass substrate and characterised with a four-point probe. The $AgGaSe_2$, Ga_2Se_3, and $AgGa_5Se_8$ films were highly resistive (more than 20 MΩ/□). The 600 nm thick Ag_2Se film had a sheet resistance of about 75 Ω/□ independent of illumination. The Ag_9GaSe_6 sample with a thickness of about 800 nm had a sheet resistance of about 5 MΩ/□. Current-voltage curves recorded with two probes separated by 3 mm on the Ag_9GaSe_6 film in dark and under 1 sun light illumination are shown in Figure S14 (the illumination level based on $AgGaSe_2$). The electrical response of the material is not trivial (not purely ohmic), but photoconductivity is evident (i.e. under illumination the apparent conductivity of the material increased by about 30%). It has to be kept in mind that the lateral conductivity may be different from the vertical conductivity due to i.e. grain boundaries. In the Ag-rich solar cell the Ag_9GaSe_6 phases that connects the front and back contacts may be free of grain boundaries (see Figure 5 in main paper). In this case one would expect a lower resistivity than implied by the measured lateral sheet resistance. In literature the resistivity of Ag_9GaSe_6 synthesised in a sealed quartz tube at 1100 °C was reported to be 8E-5 Ω*m [13]. Another study found an resistivity of 2E-4 Ω*m for stoichiometric Ag_9GaSe_6 and 2E-5 Ω*m for slightly Se poor material ($Ag_9GaSe_{5.96}$) synthesized in a quartz tube at 1000 °C [14]. A conductivity in this range can be expected for a degenerate semiconductor. The reason for the unusually high resistivity (around 4 Ω*m) for the Ag_9GaSe_6 thin film produced here remains unclear, but may relate to the different synthesis route.

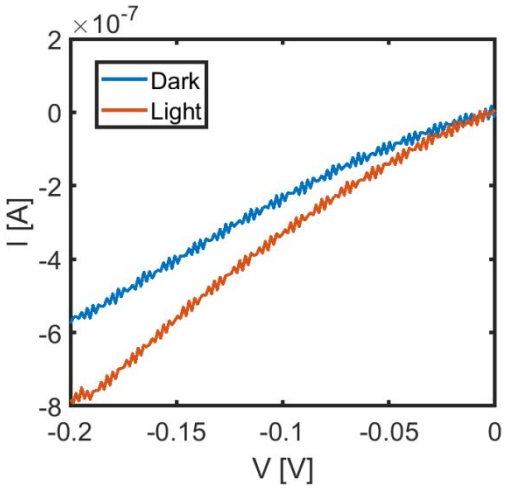

Figure S14: Current-voltage measurement of the Ag_9GaSe_6 thin film on soda-lime glass. Probes were placed 3 mm apart on the 800 nm thick film. The light curve was recorded under 1 sun illumination (the illumination level is based on $AgGaSe_2$).

5. Band gap of $AgGaSe_2$

Since a range of band gaps have been reported for $AgGaSe_2$ (1.6 [15] – 1.8eV [16]), we estimated its magnitude using three different methods. Ag-poor $AgGaSe_2$ grown with a 1-stage co-evaporation was used in all cases. The value extracted from the quantum efficiency of a device based on the maximum of the derivative is 1.76 eV (Figure 6(a) in paper)). Based on a Tauc plot for $AgGaSe_2$ on soda-lime glass obtained from spectrophotometry, the band gap is estimated to be 1.78 eV (Figure S6(b)). Likewise, energy gap of 1.78 eV is obtained from the peak position in room-temperature photoluminescence measurement (Figure S15).

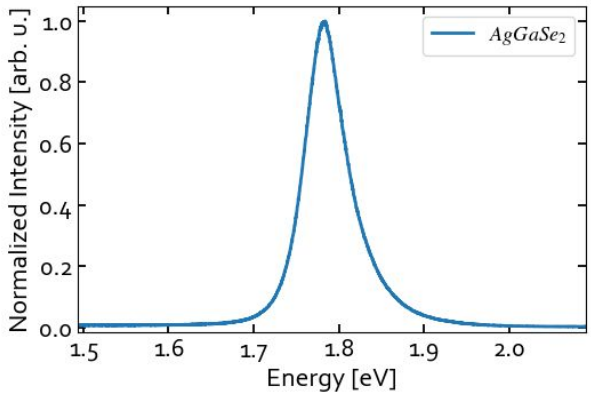

Figure S15: Room-temperature photoluminescence of the bare absorber of Ag-poor $AgGaSe_2$ grown with a 1-stage co-evaporation. The band gap is estimated to be 1.78 eV.

6. Detection of OVC in Ag-poor devices by XRD

Figure S16 shows XRD patterns measured with Bragg-Brentano (BB) and grazing incidence (GI) with incidence angle of 1 degree on the Ag-poor absorbers grown with 1- and 3-stage processes. In the BB measurement, the OVC could be identified in both samples. Using GIXRD, the peak related to the OVC is only clearly visible in the 3-stage processed device. This relates to the difference in the distribution of the OVC phases. In the 3-stage sample, OVC layers are formed at both the front and back surfaces. The surface-sensitive GIXRD is therefore capable of detecting the OVC in the surface layer. In the 1-stage process, the OVCs are located in isolated islands, with a thickness locally reduced compared to the neighbouring $AgGaSe_2$. The lower

thickness of these OVC regions may be the reason why their presence is not reflected clearly in the GIXRD measurements. It may be expected that the OVC would show up more prominently in the XRD pattern of the 3-stage process given that TEM indicates that the layer is covering the surface more or less continuously. This question will be addressed further in the section 7.

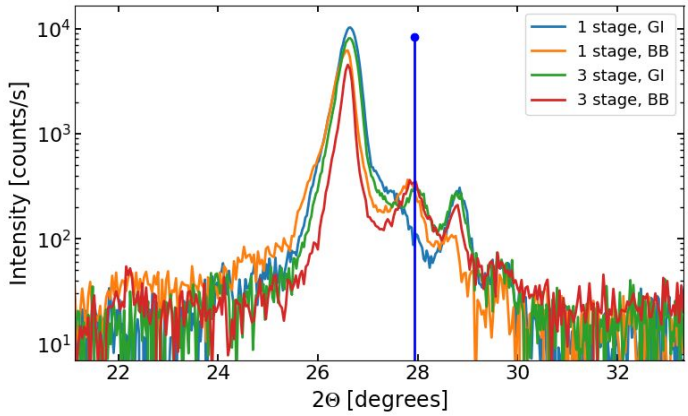

Figure S16: Bragg Brentano XRD (BB) and grazing incidence XRD (GI) with 1 degree of incidence of the Ag-poor $AgGaSe_2$ samples deposited with 1-and 3-stage processes. The vertical line indicates the reflection related to $AgGa_5Se_8$.

Figure S17 shows the result of GIXRD performed on two samples from the same deposition with integral composition of [Ag]/[Ga] = 0.22. One sample was deposited directly on SLG, while the other on Mo coated SLG. The pattern is normalized to the (112) reflection of $AgGaSe_2$. It is observed that the peak relating to the OVC phase is strongly dependent on the type of substrate. When depositing directly onto the glass substrate the reflection related to the OVC phase is strongly enhanced compared to the Mo coated sample. One possible explanation for this observation could be that supply of Na from the glass is greater when Mo is left out. The enhanced supply of Na could stabilize or catalyse the OVC formation. The exact mechanism for this observation would need further studies.

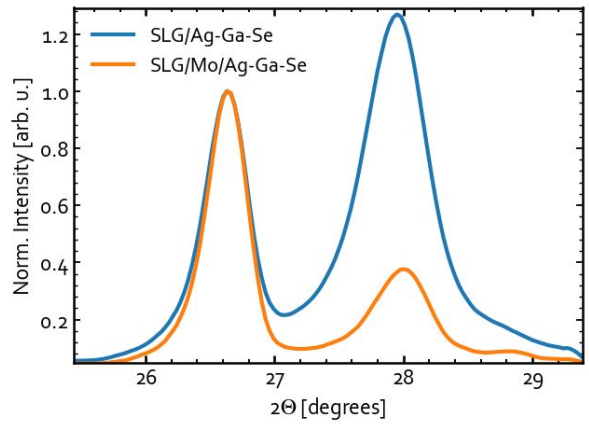

Figure S17: GIXRD (d_{inc} =1°) of two samples from the same deposition on different substrates. The spectra have been normalized to the (112) peak of $AgGaSe_2$. The sample deposited directly on SLG without Mo, has a much larger OVC peak in comparison to the sample on Mo.

7. Microstructure of devices

A few additional SEM and TEM micrographs are included in order to give a clearer comparison of the microstructure of the Ag-poor $AgGaSe_2$ samples grown with a 1- and 3-stage processes (Figure S18 and Figure S19 respectively). TEM image of the Ag-rich device is also included for comparison (Figure S20).

The imaging of the Ag-poor device produced with a 3-stage process is shown in Figure S19. It illustrates that Ag-rich particles can form under the FIB ion polishing. These could be hindered by introduction of XeF_2 during the polishing step. The fact that Ag-rich particles are absent in SEM for the cleaved sample (Figure S18) but present on the cross-section prepared with FIB suggests that these particles are not present in the as-grown materials and only emerge as a preparation and/or measurement artefact.

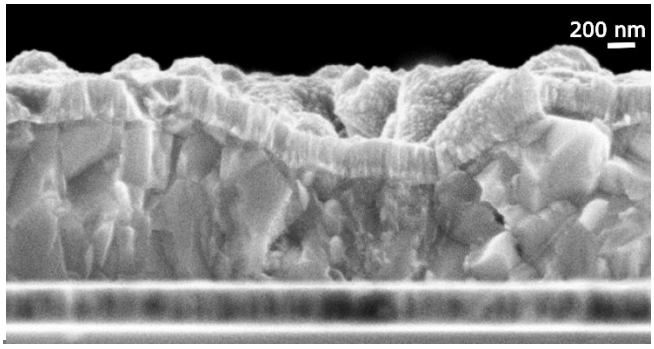

Figure S18: SEM cross-section of the Ag-poor device prepared with a 1-stage process. The region with a lower film thickness and smaller grains is the OVC phase. The surrounding film consists of chalcopyrite $AgGaSe_2$.

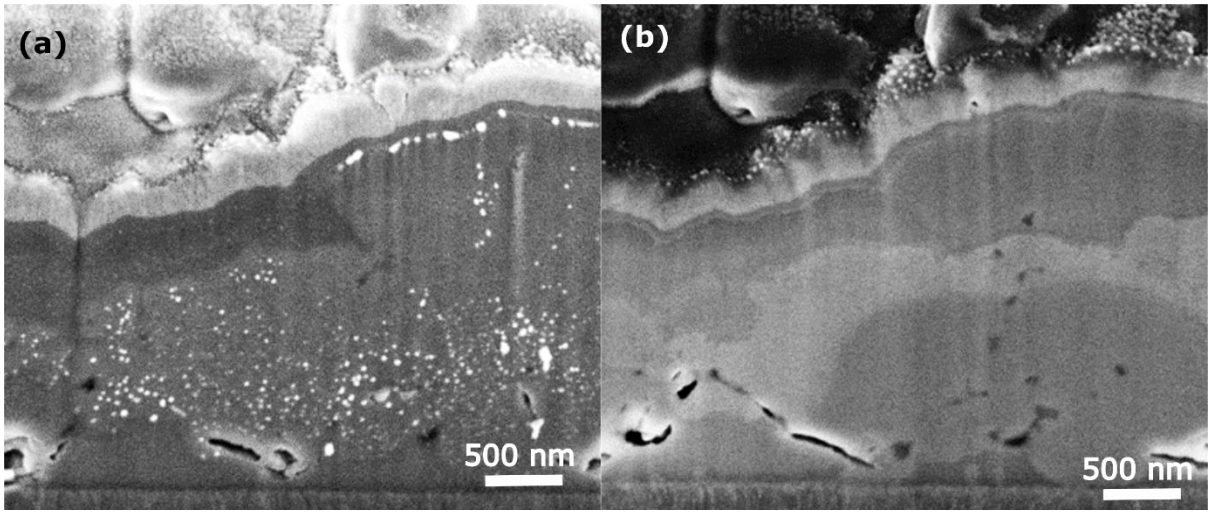

Figure S19: (a) SEM of a FIB-prepared Ag-poor $AgGaSe_2$ film grown with a 3-stage process. The bright particles are rich in Ag and form when preparing the cross-section with FIB. (b) The same cross-section slightly repolished using XeF_2-assisted milling which prevent the coalescence of the Ag-rich particles. The darker and lighter patches correspond to OVC and chalcopyrite AgGaSe2, respectively.

Close inspection of the differences between the image with and without XeF_2 in Figure S19 raises some questions. Regions with the lighter contrast and small bright particles in Figure S19(a) are likely the $AgGaSe_2$ phase, while the darker region at the back and part of the front is likely the OVC. When the bright Ag particles are forming in this region it indicates that Ag is being removed from the bulk of the material in these areas. In the dark areas these particles do not form, probably since it is harder to remove Ag from the already Ag-poor OVC. Interestingly, the introduction of XeF_2 prevent the formation of these particles, and the regions with dark contrast appeared to have increased significantly in volume compared to the lighter appearing

regions. This could be an indication that parts of the $AgGaSe_2$ has been converted to $AgGa_5Se_8$ by removal of Ag. It has to be kept in mind that the cross-section measured after XeF_2 polishing is slightly deeper in the material. By inspection of features on the surface it is clear that this will have minor effect on the observations, since the difference in depth is small. Based on the integral composition of the sample [Ag]/[Ga] = 0.81, we estimate that about 15 % of the volume should be OVC. This is fair agreement with the observation in Figure S19(a), but the amount of OVC in Figure S19(b) is significantly higher than expected. These observations question whether the $AgGaSe_2$ phase remains stable during FIB preparation, and may explain why larger than expected OVC volume fractions were observed in TEM (Figure 7 in main paper). The observation that $AgGaSe_2$ is chemically unstable is in agreement with the experience from Raman spectroscopy, where formation of amorphous Se was observed. A similar decomposition of the material may happen in both Raman and FIB/TEM investigations.

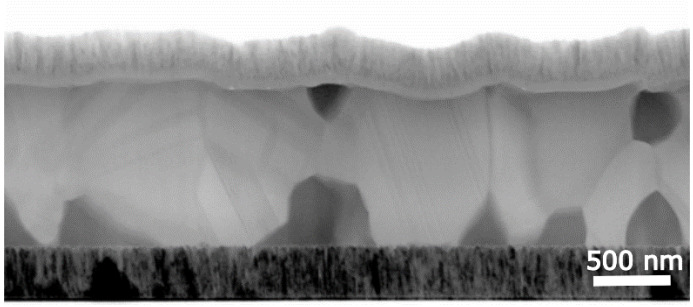

Figure S20: BF STEM of the Ag-rich $AgGaSe_2$ device. The dark areas correspond to Ag_9GaSe_6 secondary phase.

8. References

[1] J. Yu and H. Yun, "Reinvestigation of the low-temperature form of Ag_2Se (naumannite) based on single-crystal data," *Acta Crystallogr., Sect. E: Struct. Rep. Online*, vol. 67, no. 9, pp. i45–i45, 2011.

[2] J. P. Deloume, R. Faure, H. Loiseleur, and M. Roubin, "Structure Cristalline de la Phase Ag_9GaSe_6," *Acta Crystallogr., Sect. B: Struct. Crystallogr. Cryst. Chem.*, vol. 34, no. 11, pp. 3189–3193, 1978.

[3] H. Hahn, G. Frank, W. Klingler, A. D. Meyer, and G. Störger, "Untersuchungen über ternäre chalkogenide. V. Über einige ternäre chalkogenide mit chalkopyritstruktur," *Z. Anorg. Allg. Chem.*, vol. 271, pp. 153–170, 1953.

[4] D. Lübbers and V. Leute, "The crystal structure of β-Ga_2Se_3," *J. Solid State Chem.*, vol. 43, no. 3, pp. 339–345, Jul. 1982, doi: 10.1016/0022-4596(82)90250-X.

[5] H. Ishizaki *et al.*, "Structural Properties of Ag-Based Chalcopyrite Compound Thin Films for Solar Cells," *MRS Online Proc. Libr.*, vol. 865, ed 2005, doi: 10.1557/PROC-865-F5.12.

[6] P. Benoit, P. Charpin, and C. Djega-Mariadassou, "Composes Definis dans le Systeme Ag-In-Se Structure Cristalline de $AgIn_5Se_8$," *Mater. Res. Bull.*, vol. 18, no. 9, pp. 1047–1057, Sep. 1983, doi: 10.1016/0025-5408(83)90146-0.

[7] Y. Cui, U. N. Roy, P. Bhattacharya, A. Parker, A. Burger, and J. T. Goldstein, "Raman spectroscopy study of $AgGaSe_2$, $AgGa_{0.9}In_{0.1}Se_2$, and $AgGa_{0.8}In_{0.2}Se_2$ crystals," *Solid State Commun.*, vol. 150, no. 35, pp. 1686–1689, Sep. 2010, doi: 10.1016/j.ssc.2010.06.022.

[8] J. P. van der Ziel, A. E. Meixner, H. M. Kasper, and J. A. Ditzenberger, "Lattice vibrations of $AgGaS_2$, $AgGaSe_2$, and $CuGaS_2$," *Phys. Rev. B*, vol. 9, no. 10, pp. 4286–4294, May 1974, doi: 10.1103/PhysRevB.9.4286.

[9] N. Kojima, A. Yamada, K. Takahashi, T. Okamoto, M. Konagai, and K. Saito, "Photoinduced Oxidation of Epitaxial Ga_2Se_3 Grown by Molecular Beam Epitaxy," *Jpn. J. Appl. Phys.*, vol. 32, no. 7A, p. L887, Jul. 1993, doi: 10.1143/JJAP.32.L887.
[10] G. Lucovsky, A. Mooradian, W. Taylor, G. B. Wright, and R. C. Keezer, "Identification of the fundamental vibrational modes of trigonal, α - monoclinic and amorphous selenium," *Solid State Commun.*, vol. 5, no. 2, pp. 113–117, Feb. 1967, doi: 10.1016/0038-1098(67)90006-3.
[11] P. J. Carroll and J. S. Lannin, "Raman Scattering of amorphous selenium films," *Solid State Commun.*, vol. 40, no. 1, pp. 81–84, Oct. 1981, doi: 10.1016/0038-1098(81)90716-X.
[12] V. V. Poborchii, A. V. Kolobov, and K. Tanaka, "An in situ Raman study of polarization-dependent photocrystallization in amorphous selenium films," *Appl. Phys. Lett.*, vol. 72, no. 10, pp. 1167–1169, Mar. 1998, doi: 10.1063/1.121002.
[13] X. Qi *et al.*, "Thermal stability of Ag_9GaSe_6 and its potential as a functionally graded thermoelectric material," *Chem. Eng. J*, vol. 374, pp. 494–501, Oct. 2019, doi: 10.1016/j.cej.2019.05.179.
[14] B. Jiang *et al.*, "An argyrodite-type Ag_9GaSe_6 liquid-like material with ultralow thermal conductivity and high thermoelectric performance," *Chem. Commun.*, vol. 53, no. 85, pp. 11658–11661, 2017, doi: 10.1039/C7CC05935C.
[15] S. M. Patel and V. G. Kapale, "Optical properties of $AgGaSe_2$ thin films," *Thin Solid Films*, vol. 148, no. 2, pp. 143–148, Apr. 1987, doi: 10.1016/0040-6090(87)90152-0.
[16] A. Jayaraman, V. Narayanamurti, H. M. Kasper, M. A. Chin, and R. G. Maines, "Pressure dependence of the energy gap in some I-III-VI_2 compound semiconductors," *Phys. Rev. B*, vol. 14, no. 8, pp. 3516–3519, Oct. 1976, doi: 10.1103/PhysRevB.14.3516.